



CHALMERS
UNIVERSITY OF TECHNOLOGY

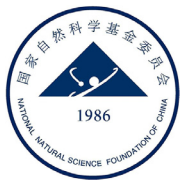
Synthetic photonic lattices based on three-level giant-atom arrays

Downloaded from: <https://research.chalmers.se>, 2026-03-07 17:54 UTC

Citation for the original published paper (version of record):

Du, L., Zhang, Y., Wang, X. et al (2026). Synthetic photonic lattices based on three-level giant-atom arrays. *Fundamental Research*, 6(1): 162-169. <http://dx.doi.org/10.1016/j.fmre.2024.03.029>

N.B. When citing this work, cite the original published paper.

Contents lists available at [ScienceDirect](#)

Fundamental Research

journal homepage: <http://www.keaipublishing.com/en/journals/fundamental-research/>

Article

Synthetic photonic lattices based on three-level giant-atom arrays

Lei Du^{a,b}, Yan Zhang^{c,*}, Xin Wang^d, Yong Li^{a,*}, Yu-xi Liu^e^a Center for Theoretical Physics & School of Physics and Optoelectronic Engineering, Hainan University, Haikou 570228, China^b Department of Microtechnology and Nanoscience, Chalmers University of Technology, Gothenburg 41296, Sweden^c School of Physics and Center for Quantum Sciences, Northeast Normal University, Changchun 130024, China^d Institute of Theoretical Physics, School of Physics, Xi'an Jiaotong University, Xi'an 710049, China^e School of Integrated Circuits, Tsinghua University, Beijing 100084, China

ARTICLE INFO

Article history:

Received 17 October 2023

Received in revised form 19 January 2024

Accepted 20 March 2024

Available online 9 May 2024

Keywords:

Giant atom

Synthetic photonic lattice

Circuit QED

Decoherence-free interaction

Quantum network engineering

ABSTRACT

Simulating photonic lattices remains to be an interesting and important goal for quantum technologies. Here, we propose several simulation schemes of one- and quasi-one-dimensional photonic lattices based on arrays of diverse three-level giant-atom dimers. The resulting models, including diamond, Su-Schrieffer-Heeger, and ladder lattices, exhibit protected nearest-neighbor and greatly inhibited next-nearest-neighbor interactions, which are challenging with most state-of-the-art experimental platforms. Our proposals based on circuit quantum electrodynamics are tunable, scalable, and reconfigurable, thus providing opportunities for simulating more advanced photonic lattices and exploring unprecedented phenomena with no counterparts in conventional condensed matter physics.

1. Introduction

Simulating the evolution of quantum particles in various periodic structures is a crucial and long-standing task in quantum mechanics, with potential applications in fields ranging from quantum many-body physics to quantum information processing. It is believed that photons are excellent quantum information carriers with low noise, long coherence length, and high transmission speed [1]. Therefore, photonic lattices provide a promising platform for engineering light-matter interactions and large-scale quantum networks, allowing for phenomena absent in conventional condensed matter physics. The research interest in photonic lattices is rising rapidly, with the implementation candidates including coupled waveguide arrays [2,3], photonic crystals [4], superconducting quantum circuits [5,6], and optomechanical systems [7–9], to name a few. Moreover, recent progress shows that it is possible to create lattice structures in synthetic dimensions, such as those based on the frequency [10–12], momentum [13], orbital angular momentum [14–16], and Fock states of photons [17]. More interestingly, it was recently shown that photonic lattices can be used to simulate curved spaces, both in real space and through a specific mapping [18,19]. These exciting breakthroughs not only find applications in computational science but also show the possibility towards unifying quantum mechanics and general relativity.

In this paper, we study a new quantum optical paradigm that allows for simulating photonic lattices with *tunable architectures and protected interactions*. The building block here is the so-called “giant atom” [20], which is coupled to a guided field at two or more separate points and can be readily implemented in experiments. Such a device can behave as a sort of tiny quantum interferometer, which exhibits self-interference effects that depend on the phase accumulations of the field traveling between different coupling points [21–26]. An important hallmark of giant atoms is their ability to interact with each other in a decoherence-free manner, i.e., the atoms exchange energy without relaxing into the waveguide field, even if the atomic frequency is within an energy band of the waveguide [27,28]. In contrast to conventional schemes where decoherence-free interactions between normal atoms (i.e., atoms that are locally coupled to the waveguide) are realized through virtual photon processes mediated by localized photon-atom bound states [29,30], in the giant-atom case the interactions can have very long range, and one does not have to engineer band gaps for the waveguide to create photon-atom bound states.

The in-band decoherence-free interactions between *two-level* giant atoms have been demonstrated to be a powerful tool for simulating one-dimensional (1D) tight-binding chains with protected and tunable nearest-neighbor couplings [27]. These couplings can be complex (i.e., mimicking synthetic magnetic flux) by properly modulating the atom-

* Corresponding authors.

E-mail addresses: zhangy345@nenu.edu.cn (Y. Zhang), yongli@hainanu.edu.cn (Y. Li).

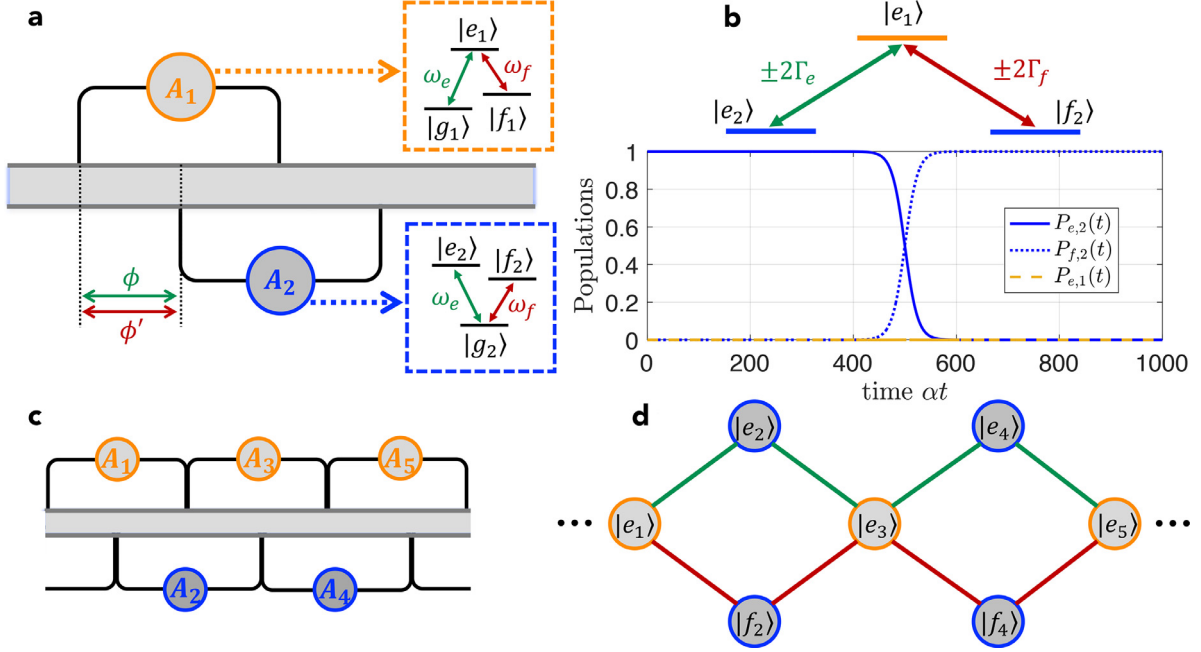


Fig. 1. (a) Schematic diagram of the $\Lambda - V$ model. The Λ - and V -type three-level giant atoms are coupled to a common 1D waveguide with an equally spaced braided structure. (b) Effective Λ -type energy-level configuration under the decoherence-free condition (upper) and the corresponding STIRAP with $n = n' = 1$, $\alpha t_1 = 400$, $\alpha t_2 = 600$, and $\alpha T = 100$ (lower). (c) $\Lambda - V$ model array with only nearest-neighbor decoherence-free interactions. (d) Effective diamond lattice based on the array in panel (c).

field interactions or the atomic transition frequencies [31]. Moreover, it is also feasible to simulate the Su-Schrieffer-Heeger (SSH) model [32,33], which is the simplest (Hermitian) topological lattice model, with two-level giant atoms based on either chiral photon-atom bound states [34] or staggered decoherence-free interactions [35]. Considering that atoms with more energy levels involved can exhibit richer quantum interference effects and more control parameters, it is natural to expect more advanced lattice structures by choosing appropriate *multi-level* giant atoms. Motivated by this, we here study several atomic dimer models based on different combinations of three-level Λ - and V -type giant atoms and demonstrate how to simulate diverse photonic lattices by extending them to well-designed arrays. Our proposals show a series of advantages compared with other conventional ones and are highly relevant to state-of-the-art experimental platforms such as superconducting quantum circuits.

The rest of this paper is organized as follows. In Section 2.1, we study an atomic dimer model consisting of a Λ - and a V -type giant atoms and then demonstrate how to simulate a diamond lattice with an array of such dimers. In Section 2.2, we study a double- Λ model and simulate the SSH model based on the extended array. In Section 2.3, we study a double- V model and construct a synthetic ladder lattice by introducing external driving fields to the extended array. In Section 3, we discuss the experimental implementations and the advantages of our proposals and conclude our work. In the supplementary material, we provide the derivation procedure of the time-delayed dynamical equations of the $\Lambda - V$ model in Section 2.1 and the analytical expressions of the eigenvalues of a more general synthetic diamond lattice, possibly with middle band gaps.

2. Results and discussion

2.1. $\Lambda - V$ model

We first consider a pair of giant atoms with Λ - and V -type three-level structures, respectively, as schematically shown in Fig. 1a. The two atoms are coupled to the waveguide in a braided structure [27,28],

with each having two identical coupling points. For simplicity, we assume that the coupling points are equally spaced by distance d , but this is not the essential condition of the results in this paper (decoherence-free interactions between giant atoms can be realized even if the braided coupling points are not equally spaced [27,28]). The Λ -type atom (labeled as A_1) has one upper state $|e_1\rangle$ and two lower states $|f_1\rangle$ and $|g_1\rangle$ (with frequencies $\omega_{e,1}$, $\omega_{f,1}$, and $\omega_{g,1}$, respectively), while the V -type atom (labeled as A_2) has two upper states $|e_2\rangle$ and $|f_2\rangle$ and one lower state $|g_2\rangle$ (with frequencies $\omega_{e,2}$, $\omega_{f,2}$, and $\omega_{g,2}$, respectively). Moreover, the energy-level transitions of the two atoms are well designed so that $\omega_{e,1} - \omega_{g,1} = \omega_{e,2} - \omega_{g,2} \equiv \omega_e$ and $\omega_{e,1} - \omega_{f,1} = \omega_{f,2} - \omega_{g,2} \equiv \omega_f$ (this condition can be appropriately relaxed as will be shown below). In experiments, such a model can be readily achieved with superconducting quantum circuit platforms, as discussed in detail in Section 3. Based on the above assumptions, the Hamiltonian of this braided $\Lambda - V$ model can be written as ($\hbar = 1$ in this paper)

$$H = H_w + H_{A_1} + H_{A_2} + V_{w1} + V_{w2}, \quad (1)$$

$$H_w = \int_{-\infty}^{+\infty} dk \omega_k a_k^\dagger a_k, \quad (2)$$

$$H_{A_1} = \omega_e |e_1\rangle\langle e_1| + \Delta_{ef} |f_1\rangle\langle f_1|, \quad (3)$$

$$H_{A_2} = \omega_e |e_2\rangle\langle e_2| + \omega_f |f_2\rangle\langle f_2|, \quad (4)$$

$$V_{w1} = \int_{-\infty}^{+\infty} dk (1 + e^{2ikd}) (g_e |e_1\rangle\langle g_1| + g_f |e_1\rangle\langle f_1|) a_k + \text{H.c.}, \quad (5)$$

$$V_{w2} = \int_{-\infty}^{+\infty} dk (e^{ikd} + e^{3ikd}) (g_e |e_2\rangle\langle g_2| + g_f |f_2\rangle\langle g_2|) a_k + \text{H.c.}, \quad (6)$$

where a_k (a_k^\dagger) is the annihilation (creation) operator of the waveguide mode with wave vector k and frequency $\omega_k = v_g |k|$ (v_g is the group velocity of the waveguide modes); g_e and g_f are the coupling coefficients between the waveguide field and the atomic transitions with frequencies ω_e and ω_f , respectively, which are assumed to be real constants

under the Weisskopf-Wigner approximation and identical for the two atoms; $\Delta_{ef} = \omega_e - \omega_f$ is the difference between the two atomic transition frequencies; and the positions of the four coupling points are assumed as $\{x_1, x_2, x_3, x_4\} = \{0, d, 2d, 3d\}$ without loss of generality. Considering that the total excitation number of the model is conserved, i.e., $[\hat{N}, H] = 0$ with $\hat{N} = \int dk a_k^\dagger a_k + |e_1\rangle\langle e_1| + |e_2\rangle\langle e_2| + |f_2\rangle\langle f_2|$ the operator of the total excitation number, and assuming that A_1 (A_2) is initially prepared in state $|e_1\rangle$ ($|g_2\rangle$), one can study the dynamics of the model in the single-excitation subspace and write the state at time t as

$$\begin{aligned} |\psi(t)\rangle = & [c_{e,1}(t)|e_1g_2\rangle + c_{e,2}(t)|g_1e_2\rangle + c_{f,2}(t)|f_1f_2\rangle]e^{-i\omega_e t}|0\rangle \\ & + \int_{-\infty}^{+\infty} dk c_k(t) a_k^\dagger e^{-i\omega_k t} |g_1g_2\rangle|0\rangle \\ & + \int_{-\infty}^{+\infty} dk c'_k(t) a_k^\dagger e^{-i\Delta_{ef}t} e^{-i\omega_k t} |f_1g_2\rangle|0\rangle, \end{aligned} \quad (7)$$

where $c_{e,1}$, $c_{e,2}$, and $c_{f,2}$ are the time-dependent probability amplitudes with the waveguide in the vacuum state $|0\rangle$ and the atomic states $|e_1\rangle$, $|e_2\rangle$, and $|f_2\rangle$ being populated, respectively; c_k (c'_k) is the time-dependent probability amplitude of creating a photon in the waveguide and atoms A_1 and A_2 in states $|g_1\rangle$ ($|f_1\rangle$) and $|g_2\rangle$, respectively. Here we have assumed that Δ_{ef} is large enough ($|\Delta_{ef}| \gg \{|g_e|, |g_f|\}$) such that a photon with frequency ω_e (ω_f) can hardly be coupled to the atomic transition of frequency ω_f (ω_e). By solving the time-dependent Schrödinger equation $i\partial_t|\psi(t)\rangle = H|\psi(t)\rangle$, one can obtain the dynamical equations:

$$i\dot{c}_{e,1}(t) = \int dk (1 + e^{2ikd}) [g_e c_k(t) e^{-i\Delta_e t} + g_f c'_k(t) e^{-i\Delta_f t}], \quad (8)$$

$$i\dot{c}_{e,2}(t) = \int dk g_e (e^{ikd} + e^{3ikd}) c_k(t) e^{-i\Delta_e t}, \quad (9)$$

$$i\dot{c}_{f,2}(t) = \int dk g_f (e^{ikd} + e^{3ikd}) c'_k(t) e^{-i\Delta_f t} \quad (10)$$

for the atomic excitation amplitudes and

$$i\dot{c}_k(t) = g_e [(1 + e^{-2ikd}) c_{e,1}(t) + (e^{-ikd} + e^{-3ikd}) c_{e,2}(t)] e^{i\Delta_e t}, \quad (11)$$

$$i\dot{c}'_k(t) = g_f [(1 + e^{-2ikd}) c_{e,1}(t) + (e^{-ikd} + e^{-3ikd}) c_{f,2}(t)] e^{i\Delta_f t} \quad (12)$$

for the field excitation amplitudes, where $\Delta_e = \omega_k - \omega_e$ and $\Delta_f = \omega_k - \omega_f$ are the detunings between waveguide mode a_k and the two atomic transitions. Assuming that the waveguide is in the vacuum state initially, it is straightforward to write down the formal solutions of $c_k(t)$ and $c'_k(t)$, i.e.,

$$c_k(t) = -i \int_0^t dt' g_e [(1 + e^{-2ikd}) c_{e,1}(t') + (e^{-ikd} + e^{-3ikd}) c_{e,2}(t')] e^{i\Delta_e t'}, \quad (13)$$

$$c'_k(t) = -i \int_0^t dt' g_f [(1 + e^{-2ikd}) c_{e,1}(t') + (e^{-ikd} + e^{-3ikd}) c_{f,2}(t')] e^{i\Delta_f t'}. \quad (14)$$

By substituting Eqs. 13 and 14 into Eqs. 8–10 and following a standard derivation procedure (for more details see Sec. I in the supplemental material), the time-delayed dynamical equations of the atomic excitation amplitudes can be obtained as

$$\begin{aligned} \dot{c}_{e,1}(t) = & -(\Gamma_e + \Gamma_f) c_{e,1}(t) - (\Gamma_e e^{2i\phi} + \Gamma_f e^{2i\phi'}) D_{e,1}^{(2)} \\ & - \frac{\Gamma_e}{2} [3e^{i\phi} D_{e,2}^{(1)} + e^{3i\phi} D_{e,2}^{(3)}] \\ & - \frac{\Gamma_f}{2} [3e^{i\phi'} D_{f,2}^{(1)} + e^{3i\phi'} D_{f,2}^{(3)}], \end{aligned} \quad (15)$$

$$\dot{c}_{e,2}(t) = -\Gamma_e [c_{e,2}(t) + e^{2i\phi} D_{e,2}^{(2)}] - \frac{\Gamma_e}{2} [3e^{i\phi} D_{e,1}^{(1)} + e^{3i\phi} D_{e,1}^{(3)}], \quad (16)$$

$$\dot{c}_{f,2}(t) = -\Gamma_f [c_{f,2}(t) + e^{2i\phi'} D_{f,2}^{(2)}] - \frac{\Gamma_f}{2} [3e^{i\phi'} D_{e,1}^{(1)} + e^{3i\phi'} D_{e,1}^{(3)}], \quad (17)$$

where $D_\beta^{(l)} = c_\beta(t-l\tau)\Theta(t-l\tau)$ with $\Theta(x)$ the Heaviside step function; $\phi = \omega_e \tau = \omega_e d/v_g$ ($\phi' = \phi - \Delta_{ef} \tau = \omega_f \tau$) is the phase accumulation of a photon with frequency ω_e (ω_f) traveling between two adjacent coupling points and τ is the corresponding time delay (i.e., propagation time); $\Gamma_e = 4\pi g_e^2/v_g$ ($\Gamma_f = 4\pi g_f^2/v_g$) is the waveguide-induced decay rate of the atomic transitions with frequency ω_e (ω_f). If we consider the situation where (i) both ϕ and ϕ' are *half-integer* multiples of π and (ii) the time delay τ is small enough such that $\{\Gamma_e \tau, \Gamma_f \tau\} \ll 1$ (i.e., in the Markovian regime), we have

$$\dot{c}_{e,1}(t) = 2 \left[(-i)^n \Gamma_e c_{e,2}(t) + (-i)^{n'} \Gamma_f c_{f,2}(t) \right], \quad (18)$$

$$\dot{c}_{e,2}(t) = 2(-i)^n \Gamma_e c_{e,1}(t), \quad (19)$$

$$\dot{c}_{f,2}(t) = 2(-i)^{n'} \Gamma_f c_{e,1}(t) \quad (20)$$

with $n = \text{mod}(\phi, 2\pi)/(\pi/2)$ and $n' = \text{mod}(\phi', 2\pi)/(\pi/2)$ (it is clear that $\{n, n'\} = \{1, 3\}$). As shown in Fig. 1b, such a model shows a protected Λ -type configuration consisting of states $|e_1\rangle$, $|e_2\rangle$, and $|f_2\rangle$, with the effective Rabi frequencies determined by the atom-waveguide coupling coefficients g_e and g_f as well as the phase accumulations ϕ and ϕ' . With this effective Λ -type configuration in hand, one can implement stimulated Raman adiabatic passage (STIRAP) [36], which enables efficient and robust population transfer from $|e_2\rangle$ to $|f_2\rangle$ (or vice versa) in a coherent control manner, by properly modulating the atom-waveguide coupling coefficients g_e and g_f (i.e., the effective Rabi frequencies Γ_e and Γ_f) with time. In circuit quantum electrodynamics (QED), such time-dependent coupling coefficients can be readily achieved by connecting the (artificial) atoms to the transmission line through superconducting quantum interference devices with tunable inductance and dynamically modulating their inductance via a controllable bias current [37]. In Fig. 1b we provide a proof-of-principle demonstration of STIRAP by using counter-intuitive time-dependent modulations $\Gamma_f(t) = \alpha \exp[-(t-t_1)^2/T^2]$ and $\Gamma_e(t) = \alpha \exp[-(t-t_2)^2/T^2]$, which show the peak value α at $t = t_1$ and $t = t_2$, respectively, and have a width $2T$ in the time domain. The adiabatic condition can be expressed as $|d\theta(t)/dt| \ll \sqrt{\Gamma_e(t)^2 + \Gamma_f(t)^2}$ with $\theta(t) = \arctan[\Gamma_e(t)/\Gamma_f(t)]$. This condition is, in principle, feasible due to the greatly suppressed decoherence of this braided giant-atom pair.

If the above $\Lambda - V$ model is extended to a multiple-atom version where an array of such atomic dimers (with an alternating arrangement of Λ - and V -type atoms) is considered to form a 1D chain, and if each atom is only braided with its two nearest neighbors but is separated from all the other atoms [27], as shown in Fig. 1c, then a 1D *diamond lattice* consisting of the atomic upper states (e.g., $|e_1\rangle$, $|e_2\rangle$, and $|f_2\rangle$) can be realized as shown in Fig. 1d.

One intriguing feature of the diamond lattice in Fig. 1d is the existence of a *flat band* [38], i.e., a completely dispersionless energy band that allows for compact localized states [39]. More specifically, the dynamical equations of such a lattice can be given by:

$$\dot{\tilde{a}}_m = -2i [\Gamma_e (\tilde{b}_m + \tilde{b}_{m-1}) + \Gamma_f (\tilde{c}_m + \tilde{c}_{m-1})], \quad (21)$$

$$\dot{\tilde{b}}_m = -2i \Gamma_e (\tilde{a}_m + \tilde{a}_{m+1}), \quad (22)$$

$$\dot{\tilde{c}}_m = -2i \Gamma_f (\tilde{a}_m + \tilde{a}_{m+1}), \quad (23)$$

where we have rewritten the atomic excitation amplitudes as $c_{e,2m-1} \rightarrow \tilde{a}_m$, $c_{e,2m} \rightarrow \tilde{b}_m$, and $c_{f,2m} \rightarrow \tilde{c}_m$ and assumed $\text{mod}(\phi, 2\pi) = \text{mod}(\phi', 2\pi) = \pi/2$. By using the plane-wave solutions $\tilde{a}_m(t), \tilde{b}_m(t), \tilde{c}_m(t) \propto \exp(ikm - iEt)$, the eigenvalues of the effective diamond lattice can be obtained as

$$E_0 = 0, \quad E_\pm = \pm 2\sqrt{2(\Gamma_e^2 + \Gamma_f^2)}(1 + \cos k), \quad (24)$$

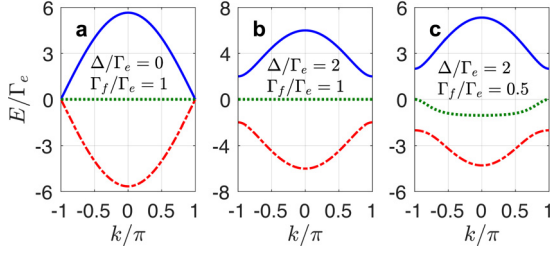


Fig. 2. Band structures of the effective diamond lattice with (a) $\Delta/\Gamma_e = 0$ and $\Gamma_f/\Gamma_e = 1$, (b) $\Delta/\Gamma_e = 2$ and $\Gamma_f/\Gamma_e = 1$, and (c) $\Delta/\Gamma_e = 2$ and $\Gamma_f/\Gamma_e = 0.5$.

which show a flat band between two symmetric dispersive ones. Note that in this case, there is no band gap between these bands, as shown in Fig. 2a.

To open band gaps, one can introduce small frequency mismatching to either the Λ -type or the V -type atom so that the transition frequencies of two atoms are not exactly matched. In fact, this is a common situation in circuit QED since it is challenging to construct exactly matched Λ - and V -type atoms (although one can also simulate the three-level structures by using two two-level atoms). Fig. 2b and c show the gapped band structures of the diamond lattice in this case (here we assume $\omega_{e,2m} - \omega_{g,2m} = \omega_e + \Delta$ and $\omega_{f,2m} - \omega_{g,2m} = \omega_f - \Delta$ with Δ the small frequency mismatching; for more details see Sec. II in the supplemental material). As expected, the frequency mismatching opens gaps between these bands, with which the associated compact localized states can be robust against certain types of disorders [40]. Note that a complete flat band disappears if $\Gamma_e \neq \Gamma_f$. As shown in Fig. 2c, although the band gaps persist in this case, the middle band is nearly dispersionless around the middle and edges of the Brillouin zone but becomes dispersive elsewhere.

2.2. Double- Λ model

In this section, we turn to consider two identical Λ -type atoms coupled to the waveguide with the equally-spaced braided structure. As shown in Fig. 3a, the Hamiltonian of such a double- Λ model can be written as $H' = H_w + H_{A_1} + H'_{A_2} + V_{w1} + V'_{w2}$, which is obtained by replacing H_{A_2} and V_{w2} in Eq. 1 by H'_{A_2} and V'_{w2} , respectively, with

$$H'_{A_2} = \omega_e |e_2\rangle\langle e_2| + \Delta_{ef} |f_2\rangle\langle f_2|, \quad (25)$$

$$V'_{w2} = \int_{-\infty}^{+\infty} dk (e^{ikd} + e^{3ikd}) (g_e |e_2\rangle\langle g_2| + g_f |e_2\rangle\langle f_2|) a_k + \text{H.c.} \quad (26)$$

If A_1 is initially prepared in state $|e_1\rangle$, there are two possible single-excitation states depending on which lower state A_2 is initially in: if A_2 is prepared in state $|g_2\rangle$ (we refer to it as “case \mathcal{A} ” hereafter), the state at time t is given by

$$\begin{aligned} |\psi(t)\rangle_{\mathcal{A}} &= [c_{e,1}(t)|e_1g_2\rangle + c_{e,2}(t)|g_1e_2\rangle] e^{-i\omega_e t} |0\rangle \\ &+ \int_{-\infty}^{+\infty} dk \left[\sum_{j=1,2} c'_{k,j}(t) |f_j\rangle\langle g_j| e^{-i\Delta_{ef} t} \right. \\ &\left. + c_{k,12}(t) \right] a_k^\dagger e^{-i\omega_k t} |g_1g_2\rangle |0\rangle, \end{aligned} \quad (27)$$

whereas if A_2 is prepared in state $|f_2\rangle$ (we refer to it as “case \mathcal{B} ” hereafter), the state becomes

$$\begin{aligned} |\psi(t)\rangle_{\mathcal{B}} &= \left\{ [c_{e,1}(t)|e_1f_2\rangle + c_{e,2}(t)|f_1e_2\rangle] e^{-i\omega_e t} \right. \\ &+ \int_{-\infty}^{+\infty} dk \left[\sum_{j=1,2} c_{k,j}(t) |g_j\rangle\langle f_j| + c'_{k,12}(t) \right. \\ &\left. \times e^{-i\Delta_{ef} t} \right] a_k^\dagger e^{-i\omega_k t} |f_1f_2\rangle \left. \right\} e^{-i\Delta_{ef} t} |0\rangle. \end{aligned} \quad (28)$$

Here $c_{k,j}(t)$ [$c'_{k,j}(t)$] is the time-dependent probability amplitude of atom A_j in state $|g\rangle$ ($|f\rangle$) and the other one in state $|f\rangle$ ($|g\rangle$), while $c_{k,12}(t)$ [$c'_{k,12}(t)$] is the time-dependent probability amplitude of both atoms in state $|g\rangle$ ($|f\rangle$). Note that the two atoms cannot be in state $|f\rangle$ ($|g\rangle$) simultaneously in case \mathcal{A} (case \mathcal{B}) during the time evolution.

By solving the time-dependent Schrödinger equation and following a similar calculation procedure as in the previous section, one can finally obtain:

$$\begin{aligned} \dot{c}_{e,1}(t) &= -(\Gamma_e + \Gamma_f)c_{e,1}(t) - (\Gamma_e e^{2i\phi} + \Gamma_f e^{2i\phi'}) D_{e,1}^{(2)} \\ &- \frac{\Gamma_e}{2} \left[3e^{i\phi} D_{e,2}^{(1)} + e^{3i\phi} D_{e,2}^{(3)} \right], \end{aligned} \quad (29)$$

$$\begin{aligned} \dot{c}_{e,2}(t) &= -(\Gamma_e + \Gamma_f)c_{e,2}(t) - (\Gamma_e e^{2i\phi} + \Gamma_f e^{2i\phi'}) D_{e,2}^{(2)} \\ &- \frac{\Gamma_e}{2} \left[3e^{i\phi} D_{e,1}^{(1)} + e^{3i\phi} D_{e,1}^{(3)} \right] \end{aligned} \quad (30)$$

in case \mathcal{A} , and obtain:

$$\begin{aligned} \dot{c}_{e,1}(t) &= -(\Gamma_e + \Gamma_f)c_{e,1}(t) - (\Gamma_e e^{2i\phi} + \Gamma_f e^{2i\phi'}) D_{e,1}^{(2)} \\ &- \frac{\Gamma_f}{2} \left[3e^{i\phi'} D_{e,2}^{(1)} + e^{3i\phi'} D_{e,2}^{(3)} \right], \end{aligned} \quad (31)$$

$$\begin{aligned} \dot{c}_{e,2}(t) &= -(\Gamma_e + \Gamma_f)c_{e,2}(t) - (\Gamma_e e^{2i\phi} + \Gamma_f e^{2i\phi'}) D_{e,2}^{(2)} \\ &- \frac{\Gamma_f}{2} \left[3e^{i\phi'} D_{e,1}^{(1)} + e^{3i\phi'} D_{e,1}^{(3)} \right] \end{aligned} \quad (32)$$

in case \mathcal{B} . Once again, in the Markovian regime of $\{\Gamma_e \tau, \Gamma_f \tau\} \ll 1$ and if $\text{mod}(\phi, 2\pi) = \text{mod}(\phi', 2\pi) = \pi/2$ (i.e., $n = n' = 1$), the above equations can be simplified to

$$\dot{c}_{e,1}(t) = -2i\Gamma_\beta c_{e,2}(t), \quad (33)$$

$$\dot{c}_{e,2}(t) = -2i\Gamma_\beta c_{e,1}(t), \quad (34)$$

where $\beta = e, f$ for cases \mathcal{A} and \mathcal{B} , respectively. Clearly, the two Λ -type atoms exhibit a decoherence-free interaction (i.e., the two atomic excited states exchange excitation without decaying into the waveguide), with the effective coupling strength depending on which state A_2 is initially prepared in. This intriguing feature allows us to implement the SSH model based on the atomic excited states. As shown in Fig. 3b, this can be accomplished by using an array of such double- Λ models, where the atoms are initially prepared in states $|g\rangle$ and $|f\rangle$ alternately.

One of the most important features of the SSH model is the existence of topologically protected edge states which are localized at the two ends of the lattice (under open boundary conditions) [41]. We plot in Fig. 4a the real-space energy spectrum of the effective SSH model, which can be described by the Hamiltonian:

$$H_{\text{SSH}} = \sum_{m=1}^M 2\Gamma_e (\hat{a}_m^\dagger \hat{b}_m + \text{H.c.}) + \sum_{m=1}^{M-1} 2\Gamma_f (\hat{b}_m^\dagger \hat{a}_{m+1} + \text{H.c.}) \quad (35)$$

with $2\Gamma_e = \Gamma_0 - \delta\Gamma$ and $2\Gamma_f = \Gamma_0 + \delta\Gamma$ describing the intracell and intercell couplings, respectively. In Eq. 35 we have defined \hat{a}_m (\hat{b}_m) as the annihilation operator of the effective lattice site $|e_{2m-1}\rangle$ ($|e_{2m}\rangle$) in the single-excitation subspace. Fig. 4a shows that a pair of zero-energy edge states appear in the middle band gap under open boundary conditions and when $\delta\Gamma$ is positive. Such a topological phase transition tends to be ideal (showing an explicit phase transition point $\delta\Gamma = 0$) in the thermodynamic limit $M \rightarrow +\infty$, as shown in the inset of Fig. 4a. These zero-energy states are protected by the chiral symmetry [42] of the lattice and thus robust against certain types of disorders.

We also examine in Fig. 4b–d the time evolutions of the initial single-site excitation $c_{e,m}(t=0) = \delta_{m,1}$ (i.e., the leftmost atom is initially prepared in state $|e\rangle$) for different values of $\delta\Gamma \in [-\Gamma_0, \Gamma_0]$. For a large (positive) $\delta\Gamma$, it shows that the excitation maintains localized in the leftmost

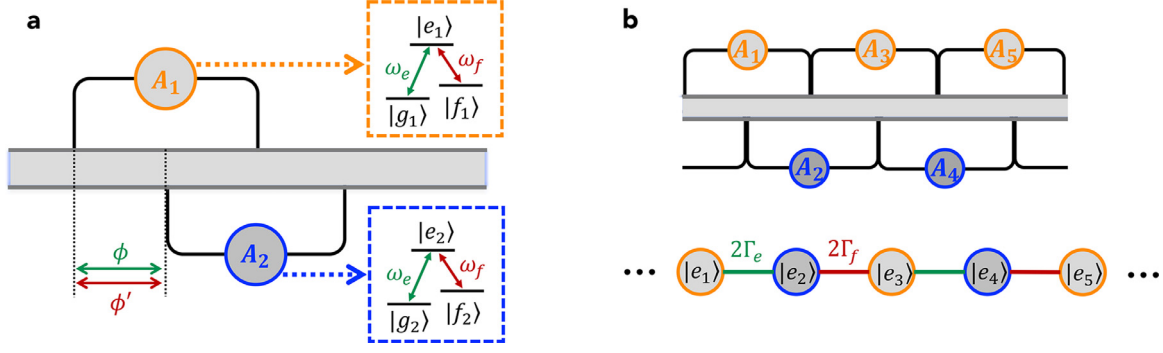


Fig. 3. (a) Schematic diagram of the double- Λ model. The two Λ -type giant atoms are coupled to a common 1D waveguide with an equally-spaced braided structure. (b) Effective SSH lattice based on an array of the double- Λ models.

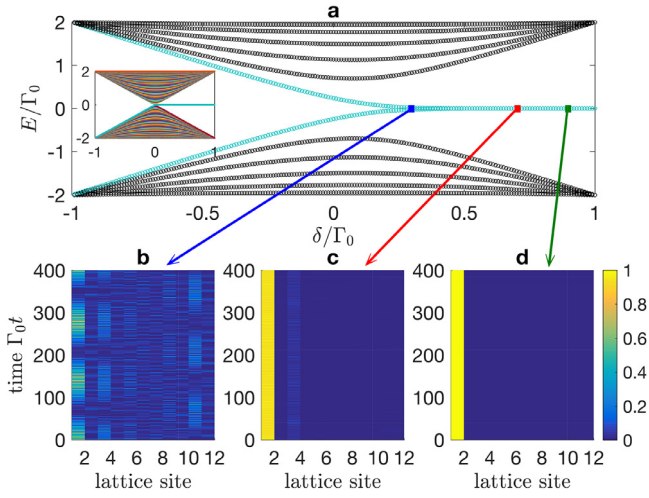


Fig. 4. (a) Energy spectrum of an effective SSH model with $M = 6$. The inset depicts the energy spectrum with $M = 50$. (b)–(d) Time evolutions of the initial single-site excitation $c_{e,m}(t=0) = \delta_{m,1}$ for (b) $\delta\Gamma/\Gamma_0 = 0.3$, (c) $\delta\Gamma/\Gamma_0 = 0.7$, and (d) $\delta\Gamma/\Gamma_0 = 0.9$. We assume $M = 6$ in panels (b)–(c). Other parameters are $\Gamma_e = (\Gamma_0 - \delta\Gamma)/2$ and $\Gamma_f = (\Gamma_0 + \delta\Gamma)/2$.

lattice site with no transfer along the lattice. As $\delta\Gamma$ decreases, the excitation may partially leak to the nearest-neighbor lattice site, which can be understood from the edge state with a weaker localization strength in this case. Such a localization feature disappears, however, when $\delta\Gamma$ becomes small enough. In this case, the excitation spreads along the lattice and is reflected back and forth by the lattice boundaries.

In contrast to the simulation scheme of SSH model based on the chiral bound states of two-level giant atoms [34], the present scheme works in a very different regime where the waveguide does not possess designed band gaps. Moreover, compared with the scheme in Ref. [35], where the SSH model is simulated based on the staggered braided structures (i.e., braided structures with designed unequal coupling separations) of two-level giant atoms, our effective SSH model is closely related to the initial states of the atoms and thus is *reconfigurable*. For instance, our model can reduce to a 1D tight-binding chain if the atoms are reset to the same lower state. Furthermore, one can also create an SSH heterostructure [43] by simply reversing the staggered atomic initial states within a chosen spatial range and engineer topologically protected interface states.

2.3. Double- V model

Finally, we study another atomic dimer model where a pair of identical V -type atoms are coupled to the waveguide with the equally-spaced

braided structure. As shown in Fig. 5a, the Hamiltonian of such a double- V model can be written as $H'' = H_w + H'_{A_1} + H_{A_2} + V'_{w1} + V_{w2}$, which is obtained by replacing H_{A_1} and V_{w1} in Eq. 1 by H'_{A_1} and V'_{w1} , respectively, with

$$H'_{A_1} = \omega_e |e_1\rangle\langle e_1| + \omega_f |f_1\rangle\langle f_1|, \quad (36)$$

$$V'_{w1} = \int_{-\infty}^{+\infty} dk (e^{ikd} + e^{3ikd}) (g_e |e_1\rangle\langle g_1| + g_f |f_1\rangle\langle g_1|) a_k + \text{H.c.} \quad (37)$$

In contrast to the case in Section 2.2, here there are two possible single-excitation states depending on which *upper* state of A_1 (i.e., $|e_1\rangle$ or $|f_1\rangle$) is initially occupied. More specifically, if A_1 is initially in state $|e_1\rangle$ (we refer to it as “case C ” hereafter), the state of the model at time t can be written as

$$|\psi(t)\rangle_C = \left\{ [c_{e,1}(t)|e_1g_2\rangle + c_{e,2}(t)|g_1e_2\rangle] e^{-i\omega_e t} + \int_{-\infty}^{+\infty} dk c_k(t) a_k^\dagger e^{-i\omega_k t} |g_1g_2\rangle \right\} |0\rangle, \quad (38)$$

whereas if A_1 is initially prepared in state $|f_1\rangle$ (we refer to it as “case D ” hereafter), the state becomes

$$|\psi(t)\rangle_D = \left\{ [c_{f,1}(t)|f_1g_2\rangle + c_{f,2}(t)|g_1f_2\rangle] e^{-i\omega_f t} + \int_{-\infty}^{+\infty} dk c_k(t) a_k^\dagger e^{-i\omega_k t} |g_1g_2\rangle \right\} |0\rangle. \quad (39)$$

Here $c_{e,j}(t)$ [$c_{f,j}(t)$] is the time-dependent probability amplitude of atom A_j in state $|e\rangle$ ($|f\rangle$) and the other one in the ground state $|g\rangle$; $c_k(t)$ is the time-dependent probability amplitude of both atoms in the ground state and creating a photon with wave vector k in the waveguide.

Once again, by solving the Schrödinger equation and following the same calculation procedure as in the previous sections, we have

$$\dot{c}_{e,1}(t) = -\Gamma_e [c_{e,1}(t) + e^{2i\phi} D_{e,1}^{(2)}] - \frac{\Gamma_e}{2} [3e^{i\phi} D_{e,2}^{(1)} + e^{3i\phi} D_{e,2}^{(3)}], \quad (40)$$

$$\dot{c}_{e,2}(t) = -\Gamma_e [c_{e,2}(t) + e^{2i\phi} D_{e,2}^{(2)}] - \frac{\Gamma_e}{2} [3e^{i\phi} D_{e,1}^{(1)} + e^{3i\phi} D_{e,1}^{(3)}] \quad (41)$$

in case C , and have:

$$\dot{c}_{f,1}(t) = -\Gamma_f [c_{f,1}(t) + e^{2i\phi'} D_{f,1}^{(2)}] - \frac{\Gamma_f}{2} [3e^{i\phi'} D_{f,2}^{(1)} + e^{3i\phi'} D_{f,2}^{(3)}], \quad (42)$$

$$\dot{c}_{f,2}(t) = -\Gamma_f [c_{f,2}(t) + e^{2i\phi'} D_{f,2}^{(2)}] - \frac{\Gamma_f}{2} [3e^{i\phi'} D_{f,1}^{(1)} + e^{3i\phi'} D_{f,1}^{(3)}] \quad (43)$$

in case D . Under the decoherence-free condition, e.g., $\text{mod}(\phi, 2\pi) = \text{mod}(\phi', 2\pi) = \pi/2$ ($n = n' = 1$), and in the Markovian regime of $\{\Gamma_e\tau, \Gamma_f\tau\} \ll 1$, we have the simplified dynamical equations:

$$\dot{c}_{\beta,1}(t) = -2i\Gamma_\beta c_{\beta,2}(t), \quad (44)$$

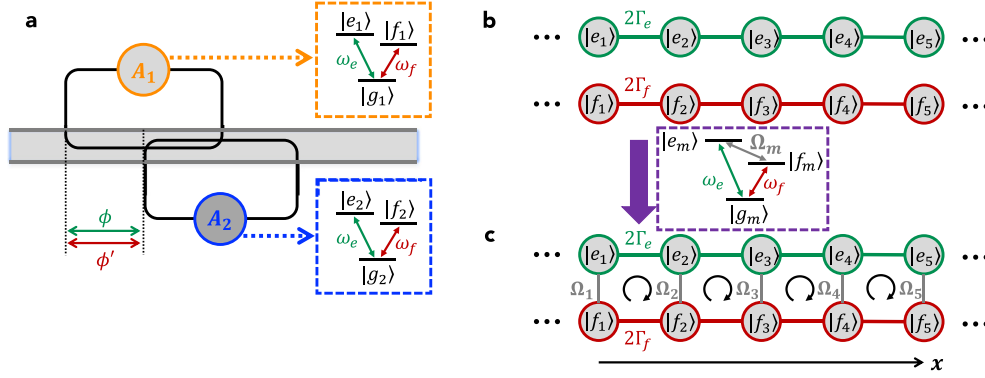


Fig. 5. (a) Schematic diagram of the double- V model. The two V -type giant atoms are coupled to a common 1D waveguide with an equally-spaced braided structure. (b) Two independent effective 1D tight-binding lattices based on an array of the double- V models. (c) Effective ladder lattice with the help of external coherent fields.

Table 1
Synthetic lattices with different giant-atom models.

Atomic pair	Effective level configuration	Atomic array
$\Lambda - V$ model	Λ -type configuration	Diamond lattice
Double- Λ model	Two-level configuration (with initial-state-dependent strength)	SSH model
Double- V model	Two-level configuration (with initial-state-dependent strength)	1D tight-binding chains (without external fields) Ladder lattice (with external fields)

$$\dot{c}_{\beta,2}(t) = -2i\Gamma_{\beta}c_{\beta,1}(t), \quad (45)$$

where $\beta = e, f$ for cases C and D , respectively. Clearly, in both cases, the two V -type giant atoms behave just like a pair of coupled two-level systems [27,28], with the effective coupling strength determined by the initial state. This implies that an array of such double- V models mimics two independent 1D tight-binding chains, as shown in Fig. 5b.

More interestingly, it is also possible to simulate a quasi-1D ladder lattice by introducing external coherent fields to drive the transitions between the two upper states $|e_m\rangle$ and $|f_m\rangle$, as shown in Fig. 5c. This is justified for three-level superconducting artificial atoms, where cyclic transition structures are allowed if the atoms are operated away from the optimal points [44,45]. Note that the cyclic structure based on an external field does not break the single-excitation assumption [24].

Such a ladder lattice can exhibit nontrivial dispersion relations if a synthetic gauge field is introduced to each square plaquette [46]. This can be achieved by introducing external fields with a phase gradient along the x direction, i.e., $\Omega_m = \Omega \exp(2im\phi)$, as shown in Fig. 5c. By performing the gauge transform $|e_m\rangle \rightarrow |e_m\rangle \exp(im\phi)$ and $|f_m\rangle \rightarrow |f_m\rangle \exp(-im\phi)$, the effective ladder lattice can be described by the Hamiltonian:

$$H_{\text{ladder}} = - \sum_m \left(\Omega \hat{a}_m^\dagger \hat{b}_m + 2\Gamma_e e^{i\phi} \hat{a}_{m+1}^\dagger \hat{a}_m + 2\Gamma_f e^{-i\phi} \hat{b}_{m+1}^\dagger \hat{b}_m + \text{H.c.} \right), \quad (46)$$

where \hat{a}_m (\hat{b}_m) now annihilates an excitation at the effective lattice site $|e_m\rangle$ ($|f_m\rangle$). Eq. 46 shows that each square plaquette of the ladder lattice is threaded by a synthetic gauge flux $\Phi = 2\phi$. By using again the plane-wave solutions $\hat{a}_m, \hat{b}_m \propto \exp(ikm - iEt)$ and assuming $2\Gamma_e = 2\Gamma_f = \Gamma$ for simplicity, the dispersion relation of the ladder lattice can be given by

$$E_{\pm} = -2\Gamma \left[\cos \phi \cos k \mp \sqrt{\sin^2 \phi \sin^2 k + \left(\frac{\Omega}{2\Gamma} \right)^2} \right]. \quad (47)$$

It is clear from Eq. 47 that the synthetic gauge field can significantly modify the dispersion relation of the lattice, leading to, e.g., the spin-momentum locking effect [46]. Moreover, one can define the average spin:

$$\langle \sigma_z \rangle_{k,\pm} = \mp \left[\cos^2 \left(\frac{\theta_k}{2} \right) - \sin^2 \left(\frac{\theta_k}{2} \right) \right] \quad (48)$$

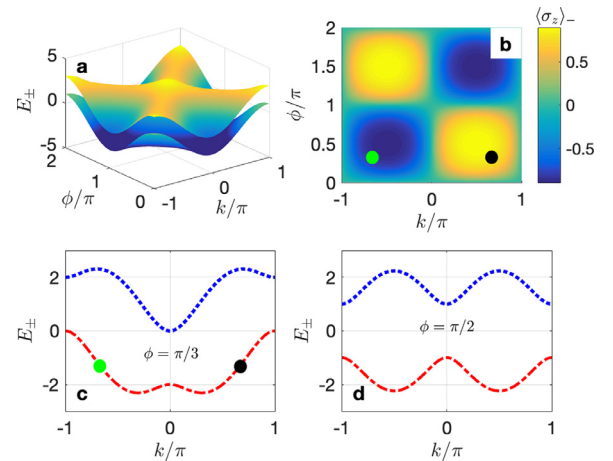


Fig. 6. (a) Energy spectrum of the ladder lattice versus k and ϕ . (b) Average spin of the lower energy band versus k and ϕ . (c) and (d) Energy band profiles versus k for (c) $\phi = \pi/3$ and (d) $\phi = \pi/2$. The filled circles in panels (b) and (c) with the same color correspond to the same parameters. In this figure we assume $\Omega = \Gamma = 1$.

for the energy bands E_{\pm} , respectively, with $\theta_k = \arctan[\Omega/(2\Gamma \sin \phi \sin k)]$. The Bloch modes of the lattice prefer to occupy the sublattice consisting of states $|e_m\rangle$ ($|f_m\rangle$) if the corresponding average spin is positive (negative).

We plot in Fig. 6 the energy bands of the ladder lattice and the average spin of the lower band to illustrate the spin-momentum locking effect mentioned above. One can find that the energy bands are closely related to the synthetic gauge flux, which allows for simulating the spin-orbital coupling [46]. As shown in Fig. 6b–d, the “spin-up” ($\langle \sigma_z \rangle_k > 0$) and “spin-down” ($\langle \sigma_z \rangle_k < 0$) modes can propagate toward opposite directions along different sublattices for appropriate values of ϕ . For example, as shown by the green and black filled circles in Fig. 6b and c, the Bloch modes with opposite wave vectors $k \approx \pm 0.665\pi$ have opposite group velocities and thus propagate toward opposite directions along

different sublattices. In this case, it is possible to observe chiral spontaneous emission of a quantum emitter if it is coupled to this lattice and resonant with one of the energy bands [46].

3. Conclusion

In conclusion, we have demonstrated a series of 1D and quasi-1D synthetic photonic lattices with protected tunnelings and nontrivial band structures. By designing pairs of Λ - and V -type three-level giant atoms, as summarized in Table 1, it is possible to create different decoherence-free level structures, which can further serve as unit cells of, e.g., diamond, SSH, and ladder lattices. More advanced lattice models can be expected by considering more types of multi-level giant atoms.

Although giant-atom systems are theoretically achievable with waveguide QED platforms based on cold atoms or various solid-state quantum emitters, it is more convenient to implement our proposals with superconducting quantum circuits where one can tune the level structure of an artificial three-level atom on demand [44,45] and the atom-field interactions can be engineered by using various tunable couplers [37,47,48]. The braided coupling structure can be easily realized by using a meandering (e.g., S -type) superconducting transmission line such that the first (second) coupling point of A_2 can be located between (outside) the two coupling points of A_1 [27,28]. In fact, a similar giant-atom system has recently been demonstrated in experiments where two frequency-tunable transmon qubits, i.e., two-level artificial atoms, are coupled to a meandering $50 - \Omega$ coplanar waveguide in the braided manner [28]. Another advantage of implementing giant-atom systems with superconducting quantum circuits is that the atom-field coupling points can be well controlled. For cold-atom platforms, however, one should consider the small oscillations of the atoms trapped in harmonic optical potentials [49]. Such oscillations may result in time-varying phase accumulations and, thereby, smeared giant-atom interference effects. Note that decoherence-free interactions between giant atoms are allowed even if the braided coupling points are not equally spaced (although the interaction strengths would be modified in this case) [27]. In practice, it is challenging to precisely control the positions of all the coupling points. This amounts to introducing tunneling disorders to the synthetic lattices. However, this is a common challenge for most existing simulation schemes. Moreover, some topologically nontrivial features, such as the edge states of the SSH model, are robust against this type of disorder since it does not break the chiral symmetry of the lattice model.

Several advantages of our proposals are summarized as follows. First, *next-nearest-neighbor couplings* are greatly inhibited due to the braided coupling structure [27]. This prevents undesired long-range interactions from smearing the synthetic lattice [50], which however remains a challenge for many other platforms [51–53]. For example, for Zigzag coupled waveguide arrays, next-nearest-neighbor couplings can be up to 30% of the nearest-neighbor ones if the intra-layer waveguide separation is twice the distance between the layers [54]. Second, for circuit QED implementations, other decay channels of the artificial atoms (such as their intrinsic dissipations into the non-guided modes of the environment) can be made very small. Therefore, using our schemes, one can construct a series of large-scale photonic lattices with, however, weak enough decoherence. Third, one can readily turn on and off the interaction between two chosen adjacent lattice sites (amounts to creating a boundary there) by tuning the corresponding atomic transitions in and out of resonance with each other. Moreover, some of the schemes proposed in this paper (e.g., those based on the double- Λ and double- V models) are *reconfigurable*. One can simulate different lattice models by changing the initial states of the atoms without reconstructing the architecture of the system. Last but not the least, although we have focused on decoherence-free interactions in this paper, controllable dissipations (into the waveguide) can be introduced to the atoms (i.e., the lattice sites) by tuning the coupling separations of the braided structure. This provides the possibility to simulate non-Hermitian photonic lattices with structured loss [55].

Declaration of competing interest

The authors declare that they have no conflicts of interest in this work.

CRediT authorship contribution statement

Lei Du: Investigation, Methodology, Writing – original draft. **Yan Zhang:** Funding acquisition, Supervision, Writing – review & editing. **Xin Wang:** Methodology, Validation. **Yong Li:** Funding acquisition, Supervision, Writing – review & editing. **Yu-xi Liu:** Supervision, Project administration, Writing – review & editing.

Acknowledgments

This work is supported by the National Natural Science Foundation of China (12274107, 12074030, 12174303, and 11804270), the Fundamental Research Funds for the Central Universities (xzy012023053), and the Key-Area Research and Development Program of Guangdong Province (2018B030326001).

Supplementary material

Supplementary material associated with this article can be found, in the online version, at doi:10.1016/j.fmre.2024.03.029.

References

- [1] J.L. O'Brien, A. Furusawa, J. Vučković, Photonic quantum technologies, *Nat. Photon.* 3 (2009) 687.
- [2] D.N. Christodoulides, F. Lederer, Y. Silberberg, Discretizing light behaviour in linear and nonlinear waveguide lattices, *Nature* 424 (2003) 817.
- [3] M.C. Rechtsman, J.M. Zeuner, Y. Plotnik, et al., Photonic floquet topological insulators, *Nature* 496 (2013) 196.
- [4] T. Ochiai, M. Onoda, Photonic analog of graphene model and its extension: Dirac cone, symmetry, and edge states, *Phys. Rev. B* 80 (2009) 155103.
- [5] M.J. Hartmann, F.G.S.L. Brandão, M.B. Plenio, Quantum many-body phenomena in coupled cavity arrays, *Laser Photon. Rev.* 2 (2008) 527.
- [6] G.P. Fedorov, S.V. Remizov, D.S. Shapiro, et al., Photon transport in a Bose-Hubbard chain of superconducting artificial atoms, *Phys. Rev. Lett.* 126 (2021) 180503.
- [7] M. Schmidt, S. Kessler, V. Peano, et al., Optomechanical creation of magnetic fields for photons on a lattice, *Optica* 2 (2015) 635.
- [8] V. Peano, C. Brendel, M. Schmidt, et al., Topological phases of sound and light, *Phys. Rev. X* 5 (2015) 031011.
- [9] A. Youssefi, S. Kono, A. Bancora, et al., Topological lattices realized in superconducting circuit optomechanics, *Nature* 612 (2022) 666.
- [10] L. Yuan, Q. Lin, M. Xiao, et al., Synthetic dimension in photonics, *Optica* 5 (2018) 1396.
- [11] C. Qin, F. Zhou, Y. Peng, et al., Spectrum control through discrete frequency diffraction in the presence of photonic gauge potentials, *Phys. Rev. Lett.* 120 (2018) 133901.
- [12] J.S.C. Hung, J.H. Busnaina, C.W.S. Chang, et al., Quantum simulation of the bosonic Creutz ladder with a parametric cavity, *Phys. Rev. Lett.* 127 (2021) 100503.
- [13] D.-W. Wang, R.-B. Liu, S.-Y. Zhu, et al., Superradiance lattice, *Phys. Rev. Lett.* 114 (2015) 043602.
- [14] X.-W. Luo, X. Zhou, C.-F. Li, et al., Quantum simulation of 2D topological physics in a 1d array of optical cavities, *Nat. Commun.* 6 (2015) 7704.
- [15] X.-W. Luo, X. Zhou, J.-S. Xu, et al., Synthetic-lattice enabled all-optical devices based on orbital angular momentum of light, *Nat. Commun.* 8 (2017) 16097.
- [16] L. Yuan, Q. Lin, A. Zhang, et al., Photonic gauge potential in one cavity with synthetic frequency and orbital angular momentum dimensions, *Phys. Rev. Lett.* 122 (2019) 083903.
- [17] J. Deng, H. Dong, C. Zhang, et al., Observing the quantum topology of light, *Science* 378 (2022) 966.
- [18] A.J. Kollár, M. Fitzpatrick, A.A. Houck, Hyperbolic lattices in circuit quantum electrodynamics, *Nature* 571 (2019) 45.
- [19] C. Lv, R. Zhang, Z. Zhai, et al., Curving the space by non-hermiticity, *Nat. Commun.* 13 (2022) 2184.
- [20] A.F. Kockum, Quantum optics with giant atoms—the first five years, in: M. Wakayama (Ed.), *Mathematics for Industry*, Springer, Singapore, 2021, pp. 125–146.
- [21] L. Guo, A. Grimsmo, A.F. Kockum, et al., Giant acoustic atom: A single quantum system with a deterministic time delay, *Phys. Rev. A* 95 (2017) 053821.
- [22] G. Andersson, B. Suri, L. Guo, et al., Non-exponential decay of a giant artificial atom, *Nat. Phys.* 15 (2019) 1123.
- [23] W. Zhao, Z. Wang, Single-photon scattering and bound states in an atom-waveguide system with two or multiple coupling points, *Phys. Rev. A* 101 (2020) 053855.
- [24] L. Du, Y. Zhang, J.-H. Wu, et al., Giant atoms in a synthetic frequency dimension, *Phys. Rev. Lett.* 128 (2022) 223602.

- [25] Z.-Q. Wang, Y.-P. Wang, J. Yao, et al., Giant spin ensembles in waveguide magnonics, *Nat. Commun.* 13 (2022) 7580.
- [26] A. Soro, C.S. Muñoz, A.F. Kockum, Interaction between giant atoms in a one-dimensional structured environment, *Phys. Rev. A* 107 (2023) 013710.
- [27] A.F. Kockum, G. Johansson, F. Nori, Decoherence-free interaction between giant atoms in waveguide quantum electrodynamics, *Phys. Rev. Lett.* 120 (2018) 140404.
- [28] B. Kannan, M. Ruckriegel, D. Campbell, et al., Waveguide quantum electrodynamics with superconducting artificial giant atoms, *Nature* 583 (2020) 775.
- [29] J.S. Douglas, H. Habibian, C.-L. Hung, et al., Quantum many-body models with cold atoms coupled to photonic crystals, *Nat. Photon.* 9 (2015) 326.
- [30] D.E. Chang, J.S. Douglas, A. González-Tudela, et al., Colloquium: Quantum matter built from nanoscopic lattices of atoms and photons, *Rev. Mod. Phys.* 90 (2018) 031002.
- [31] L. Du, L. Guo, Y. Li, Complex decoherence-free interactions between giant atoms, *Phys. Rev. A* 107 (2023) 023705.
- [32] W.P. Su, J.R. Schrieffer, A.J. Heeger, Solitons in polyacetylene, *Phys. Rev. Lett.* 42 (1979) 1698.
- [33] A.J. Heeger, S. Kivelson, J.R. Schrieffer, et al., Solitons in conducting polymers, *Rev. Mod. Phys.* 60 (1988) 781.
- [34] X. Wang, T. Liu, A.F. Kockum, et al., Tunable chiral bound states with giant atoms, *Phys. Rev. Lett.* 126 (2020) 043602.
- [35] Y.P. Peng, W.Z. Jia, Single-photon scattering from a chain of giant atoms coupled to a one-dimensional waveguide, *Phys. Rev. A* 108 (2023) 043709.
- [36] P. Marte, P. Zoller, J.L. Hall, Coherent atomic mirrors and beam splitters by adiabatic passage in multilevel systems, *Phys. Rev. A* 44 (1991). R4118(R)
- [37] Y. Yin, Y. Chen, D. Sank, et al., Catch and release of microwave photon states, *Phys. Rev. Lett.* 110 (2013) 107001.
- [38] D. Leykam, S. Flach, Perspective: Photonic flatbands, *APL Photonics* 3 (2018) 070901.
- [39] R. Khomeriki, S. Flach, Landau-Zener Bloch oscillations with perturbed flat bands, *Phys. Rev. Lett.* 116 (2016) 245301.
- [40] D. Leykam, J.D. Bodyfelt, A.S. Desyatnikov, et al., Localization of weakly disordered flat band states, *Eur. Phys. J. B* 90 (2017) 1.
- [41] J.K. Asboth, L. Oroszlany, A. Palyi, *A Short Course on Topological Insulators*, Springer International, Cham, 2016.
- [42] A.P. Schnyder, S. Ryu, A. Furusaki, et al., Classification of topological insulators and superconductors in three spatial dimensions, *Phys. Rev. B* 78 (2008) 195125.
- [43] L. Du, J.-H. Wu, M. Artoni, et al., Phase-dependent topological interface state and spatial adiabatic passage in a generalized Su-Schrieffer-Heeger model, *Phys. Rev. A* 100 (2019) 012112.
- [44] Y.X. Liu, J.Q. You, L.F. Wei, et al., Optical selection rules and phase-dependent adiabatic state control in a superconducting quantum circuit, *Phys. Rev. Lett.* 95 (2005) 087001.
- [45] X. Gu, A.F. Kockum, A. Miranowicz, et al., Microwave photonics with superconducting quantum circuits, *Phys. Rep.* 718 (2017) 1.
- [46] X. Wang, Z.-M. Gao, J.-Q. Li, et al., Unconventional quantum electrodynamics with a Hofstadter-ladder waveguide, *Phys. Rev. A* 106 (2022) 043703.
- [47] M.R. Geller, E. Donate, Y. Chen, et al., Tunable coupler for superconducting Xmon qubits: Perturbative nonlinear model, *Phys. Rev. A* 92 (2015) 012320.
- [48] M. Kounalakis, C. Dickel, A. Bruno, et al., Tuneable hopping and nonlinear cross-kerr interactions in a high-coherence superconducting circuit, *njp Quantum Inf.* 4 (2018) 38.
- [49] I. Iorsh, A. Poshakinskiy, A. Poddubny, Waveguide quantum optomechanics: Parity-time phase transitions in ultrastrong coupling regime, *Phys. Rev. Lett.* 125 (2020) 183601.
- [50] J.-Q. Li, Z.-M. Gao, W.-X. Liu, et al., Light-matter interactions in a Hofstadter lattice with next-nearest-neighbor couplings, *Phys. Rev. A* 108 (2023) 043708.
- [51] A.H.C. Neto, F. Guinea, N.M.R. Peres, et al., The electronic properties of graphene, *Rev. Mod. Phys.* 81 (2009) 109.
- [52] P. Richerme, Z.-X. Gong, A. Lee, et al., Non-local propagation of correlations in quantum systems with long-range interactions, *Nature* 511 (2014) 98.
- [53] D. Barredo, H. Labuhn, S. Ravets, et al., Coherent excitation transfer in a spin chain of three Rydberg atoms, *Phys. Rev. Lett.* 114 (2015) 113002.
- [54] F. Dreisow, A. Szameit, M. Heinrich, et al., Second-order coupling in femtosecond-laser-written waveguide arrays, *Opt. Lett.* 33 (2008) 2689.
- [55] F. Roccati, S. Lorenzo, G. Calajò, et al., Exotic interactions mediated by a non-hermitian photonic bath, *Optica* 9 (2022) 565.

Author profile

Lei Du is currently a postdoctoral researcher of Prof. Janine Splettstoesser's group at the Department of Microtechnology and Nanoscience (MC2), Chalmers University of Technology. He is now working on a number of fields of quantum optics and condensed matter physics, including waveguide quantum electrodynamics, cavity optomechanics, and topological photonics.

Yan Zhang (BRID: 03105.00.21720) is an associate professor of School of Physics and the deputy director of the National Demonstration Center for Experimental Physics Education at Northeast Normal University. He is a theoretical physicist working on various aspects of quantum optics and non-Hermitian optics, including quantum interference effect, cavity optomechanics, giant atom, and PT-symmetric optics. He received the Ph.D. degree in optics from Jilin University.

Yong Li is a professor of physics at School of Physics and Optoelectronic Engineering, the vice director of Center for Theoretical Physics in Hainan University. His research interests include the optomechanics, giant atoms, and optics-assisted enantio-detection of chiral molecules. His works have been published in *Physical Review Letters*, *Journal of Physical Chemistry Letters*, and other journals. He has won the Excellent Young Scientists Fund of the National Natural Science Foundation of China.